Experimental studies of guided wave damage identification in beams using a probabilistic approach

*Ching-Tai Ng[1]

[1] *School of Civil, Environmental & Mining Engineering, The University of Adelaide, SA, 5005, Australia*
[1] *alex.ng@adelaide.edu.au*

ABSTRACT

This paper presents an experimental study of quantitative identification of damages in beams using guided wave. A Bayesian probabilistic approach is proposed to identify the damage location, length and depth. The damage identification is achieved by solving an optimization problem, in which the probability density function (PDF) of the damage parameters is maximized. In this study a hybrid particle swarm optimization (HPSO) algorithm is employed to guarantee the global optimum solution. One advantage of the proposed methodology is that the Bayesian approach not only pinpoints the location, length and depth of the damage, but also quantifies the uncertainties associated with the damage identification results through calculating the posterior PDF of the identified damage parameters. This provides essential information for making decisions on necessary remedial work. In the experimental study a piezoceramic transducer is used for excitation. The guided wave signals are then measured using a laser Doppler vibrometer system. Metallic beams with different damage configurations are considered in the experimental verification.

1. INTRODUCTION

Beams are commonly used as structural components in different engineering structures, such as civil and mechanical engineering. Existence of damages in structural components can potentially lead to failure of structures. In the last decade various damage detection methods (Kim *et al*. 2004; Lam *et al*. 2008; Rosales *et al*. 2009) have been developed to ensure the safety and reduce the maintenance costs of structures. In recent years guided wave has been recognized as one of the promising methods for damage detection. It requires a high frequency excitation to generate pulses or wave packets propagating in structures. The main advantages of guided wave are its high sensitive to small damages (Ng & Veidt 2011; Veidt & Ng 2011) and large inspection region with a small number of transducers.

Different methods have been developed to detect damages in structures using guided wave. Nag *et al*. (2002) proposed a model-based approach to identify delaminations in composite beams. Genetic algorithm was used to update a damaged

---

[1] Lecturer

spectral element model for damage identification. The proposed method was verified using numerical simulations. Krawczuk (2002) employed a genetic algorithm gradient technique for crack identification in beams. The feasibility and capability of the proposed method was demonstrated through numerical case studies. Liew and Veidt (2009) applied artificial neural network to identify damage in beams. Wavelet decomposition was used to construct pattern features for damage identification using the artificial neural network. The proposed method was investigated through experimental case studies. Ng *et al.* (2009) proposed a probabilistic optimization approach to identify damages in beams. The simulated annealing was employed as the optimization algorithm in damage detection. Comprehensive numerical case studies were used to investigate the performance of the proposed method in identifying damages with different sizes and under different measurement noises. Rucka (2010) numerically and experimentally investigated the wave propagation in a damaged beam. A method was proposed to detect damages by analyzing wave speeds and reflected waves from the damages. Pau and Vestroni (2011) proposed a damage identification approach using longitudinal wave propagation. Damages were identified by comparing the analytical and measured time histories of the exited waves. The proposed approach was verified through numerical and experiment studies.

In this study a probabilistic approach is proposed to identify damages in beams. The proposed method is a model-based approach, which combines a numerical simulation model and a probabilistic model. Hence it is not only able to provide quantitative information of the damages but also quantifies the uncertainties associated with the damage identification results, which provides essential information for making decisions about necessary remedial work. The proposed approach is able to achieve the damage identification with only one single measurement point, which significantly reduces the cost of the damage detection process. In the proposed method a damaged beam model is developed using a computationally efficient frequency domain spectral finite element method based on the Mindlin-Hermann theory. The damage identification is achieved by maximizing the posterior probability density function (PDF) of damage parameters. A hybrid optimization method, which combines the particle swarm optimization algorithm, is proposed to enhance the reliability and efficiency in determining the global optimum. One of the objectives of this study is to provide an experimental verification for the proposed damage identification method.

The organization of the paper is as follows. The frequency domain spectral finite element method based on the Mindlin-Hermann theory is presented in Section 2, along with a throw-off element for modeling semi-infinite and infinite beams, and the modeling of the damaged beam. The proposed probabilistic approach is then presented in Section 3. The details of the experimental verification are provided in Section 4. Finally, conclusions are drawn in Section 5.

2. Spectral Finite Element Method

The longitudinal guided wave propagation in beam-type structures can be modeled using a number of frequency domain spectral finite elements based on Mindlin-

Herrmann theory. The theory takes into account independent shearing deformation of longitudinal guided wave propagation. A j-th frequency domain spectral finite element with length L_j has two nodal points located at left and right ends of the beam, respectively. Each nodal point has two degrees-of-freedom, a longitudinal displacement and a rotation, which describes the transverse contraction of longitudinal guided wave propagation. The governing equations (Doyle1997; Krawczuk *et al.* 2006) are

$$\left(2\mu_j + \lambda_j\right)A_j \frac{\partial^2 \bar{u}_j}{\partial x^2} + \lambda_j A_j \frac{\partial \bar{\phi}_j}{\partial x} = \rho_j A_j \frac{\partial^2 \bar{u}_j}{\partial t^2} \tag{1}$$

$$\mu_j I_j S_1 \frac{\partial^2 \bar{\phi}_j}{\partial x^2} - \left(2\mu_j + \lambda_j\right)A_j \bar{\phi}_j - \lambda_j A_j \frac{\partial \bar{u}_j}{\partial x} = \rho_j I_j S_{2,j} \frac{\partial^2 \bar{\phi}_j}{\partial t^2} \tag{2}$$

where $\bar{u}_j$ and $\bar{\phi}_j$ are the horizontal displacement and rotational angle on the neutral axis of the beam. E_j and v_j are the Young's modulus and Poisson's ratio, respectively. b_j and h_j are the width and thickness of the beam. $A_j = b_j h_j$ and $I_j = b_j h_j^3 / 12$ are the cross-section area and second moment of area of the beam. $\mu_j = E_j / (2(1 + v_j))$ and $\lambda_j = v_j E_j / ((1 + v_j)(1 - 2v_j))$ are Lame constants. ρ_j is the density. $S_1 = 12 / \pi^2$ and $S_{2,j} = S_1 ((1 + v_j) / (0.87 + 1.12 v_j))^2$ are correction factors (Doyle 1997). The spectral representations for $\bar{u}_j$ and $\bar{\phi}_j$ are

$$\bar{u}_j(x,t) = \sum_{n=1}^{N} \hat{u}_{n,j}(x,\omega_n) e^{i\omega_n t}, \qquad \bar{\phi}_j(x,t) = \sum_{n=1}^{N} \hat{\phi}_{n,j}(x,\omega_n) e^{i\omega_n t} \tag{3}$$

where $\hat{u}_{n,j}$ and $\hat{\phi}_{n,j}$ are the Fourier coefficients associated with the responses variable $\bar{u}_j$ and $\bar{\phi}_j$ at *n*-th angular frequency ω_n. ω_N is the Nyquist frequency and i is the imaginary unit. The spectrum relation of the dependent variable $\hat{u}_j$ and $\hat{\phi}_j$ can be obtained by assuming solutions in the forms

$$\hat{u}_{n,j}(x,\omega_n) = U_j e^{-i(k_j x - \omega_n t)}, \qquad \hat{\phi}_{n,j}(x,\omega_n) = \Phi_j e^{-i(k_j x - \omega_n t)} \tag{4}$$

where k_j is the wavenumber corresponding to ω_n. U_j and Φ_j are amplitude spectrums at *n*-th angular frequency. Substituting Eqs. (3) and (4) into the differential governing equation, the characteristic equation for the solution of the wavenumber can be obtained as

$$\left\{ k_j^2 \mathbf{B}_{2,j} + k_j \mathbf{B}_{1,j} + \mathbf{B}_{0,j} \right\} \begin{Bmatrix} R_{1,j} \\ R_{2,j} \end{Bmatrix} = 0 \tag{5}$$

where

$$\mathbf{B}_{0,j} = \begin{bmatrix} \rho_j A_j \omega_n^2 & 0 \\ 0 & -\left(2\mu_j + \lambda_j\right)A_j + \rho_j I_j S_{2,j}\omega_n^2 \end{bmatrix} \tag{6}$$

$$\mathbf{B}_{1,j} = \begin{bmatrix} 0 & -ik_j\lambda_j A_j \\ ik_j\lambda_j A_j & 0 \end{bmatrix} \tag{7}$$

$$\mathbf{B}_{2,j} = \begin{bmatrix} -\left(2\mu_j + \lambda_j\right)A_j & 0 \\ 0 & -\mu_j I_j S_1 \end{bmatrix} \tag{8}$$

Eq. (5) is a second order standard polynomial eigenvalue problem and there are four eigenvalues k_j and eigenvectors $\{U_j \quad \Phi_j\}^T$. Using the QZ algorithm (Jean-Pierre & Tisseur 2003) and arranging eigenvectors in a matrix $\mathbf{R}$, the general solution at frequency ω_n is

$$\begin{Bmatrix} \hat{u}_{n,j}(x) \\ \hat{\phi}_{n,j}(x) \end{Bmatrix} = \sum_{m=1}^{2} C_{m,j} \begin{Bmatrix} R_{1m,j} \\ R_{2m,j} \end{Bmatrix} e^{-ik_{m,j}x} + \sum_{m=3}^{4} C_{m,j} \begin{Bmatrix} R_{1m,j} \\ R_{2m,j} \end{Bmatrix} e^{ik_{m,j}(L_j-x)} \tag{9}$$

where $C_{m,j}$ are unknown coefficients to be found from the nodal conditions at $x = 0$ and $x = L_j$ as

$$\hat{u}_{n,j}(0) = \hat{u}_{\alpha,j}, \quad \hat{\phi}_{n,j}(0) = \hat{\phi}_{\alpha,j}, \quad \hat{u}_{n,j}(L_j) = \hat{u}_{\beta,j}, \quad \hat{\phi}_{n,j}(L_j) = \hat{\phi}_{\beta,j} \tag{10}$$

The relation between the spectral longitudinal displacement and lateral contraction with the unknown coefficient $C_{m,j}$ is

$$\boldsymbol{\delta}_j = \mathbf{T}_{1,j}\mathbf{C}_j \tag{11}$$

where

$$\boldsymbol{\delta}_j = \left\{ \hat{u}_{\alpha,j} \quad \hat{\phi}_{\alpha,j} \quad \hat{u}_{\beta,j} \quad \hat{\phi}_{\beta,j} \right\}^T \tag{12}$$

$$\mathbf{C}_j = \left\{ C_{1,j} \quad C_{2,j} \quad C_{3,j} \quad C_{4,j} \right\}^T \tag{13}$$

$$\mathbf{T}_{1,j} = \begin{bmatrix} R_{11,j} & R_{12,j} & R_{13,j}e^{ik_{3,j}L_j} & R_{14,j}e^{ik_{4,j}L_j} \\ R_{21,j} & R_{22,j} & R_{23,j}e^{ik_{3,j}L_j} & R_{24,j}e^{ik_{4,j}L_j} \\ R_{11,j}e^{-ik_{1,j}L_j} & R_{12,j}e^{-ik_{2,j}L_j} & R_{13,j} & R_{14,j} \\ R_{21,j}e^{-ik_{1,j}L_j} & R_{22,j}e^{-ik_{2,j}L_j} & R_{23,j} & R_{24,j} \end{bmatrix} \tag{14}$$

The forces at the nodal spectral axial and shear forces at left and right ends are

$$\hat{F}_{\alpha,j} = -\left[\left(2\mu_j + \lambda_j \right) A_j \frac{\partial \hat{u}_j \left(0, \omega_n \right)}{\partial x} + \lambda_j A_j \hat{\phi}_j \left(0, \omega_n \right) \right], \quad \hat{Q}_{\alpha,j} = -\mu_j I_j S_1 \frac{\partial \hat{\phi}_j \left(0, \omega_n \right)}{\partial x} \quad (15)$$

$$\hat{F}_{\beta,j} = -\left[\left(2\mu_j + \lambda_j \right) A_j \frac{\partial \hat{u}_j \left(0, \omega_n \right)}{\partial x} + \lambda_j A_j \hat{\phi}_j \left(0, \omega_n \right) \right], \quad \hat{Q}_{\beta,j} = -\mu_j I_j S_1 \frac{\partial \hat{\phi}_j \left(0, \omega_n \right)}{\partial x} \quad (16)$$

and they can be related to the unknown coefficient matrix $\mathbf{C}_j$ as

$$\mathbf{F}_j = \mathbf{T}_{2,j} \mathbf{C}_j \quad (17)$$

where

$$\mathbf{F}_j = \left\{ \hat{F}_{\alpha,j} \quad \hat{Q}_{\alpha,j} \quad \hat{F}_{\beta,j} \quad \hat{Q}_{\beta,j} \right\}^T \quad (18)$$

$$\mathbf{T}_{2,j} = \begin{bmatrix} ik_{1,j}\Delta_{1,j}R_{11,j} - \Delta_{2,j}R_{21,j} & ik_{2,j}\Delta_{1,j}R_{12,j} - \Delta_{2,j}R_{22,j} & \left(ik_{3,j}\Delta_{1,j}R_{13,j} - \Delta_{2,j}R_{23,j} \right)e^{ik_{3,j}L_j} & \left(ik_{4,j}\Delta_{1,j}R_{14,j} - \Delta_{2,j}R_{24,j} \right)e^{ik_{4,j}L_j} \\ ik_{1,j}\Delta_{3,j}R_{21,j} & ik_{2,j}\Delta_{3,j}R_{22,j} & ik_{3,j}\Delta_{3,j}R_{23,j}e^{ik_{3,j}L_j} & ik_{4,j}\Delta_{3,j}R_{24,j}e^{ik_{4,j}L_j} \\ \left(-ik_{1,j}\Delta_{1,j}R_{11,j} + \Delta_{2,j}R_{21,j} \right)e^{-k_{1,j}L_j} & \left(-ik_{2,j}\Delta_{1,j}R_{12,j} + \Delta_{2,j}R_{22,j} \right)e^{-k_{2,j}L_j} & -ik_{3,j}\Delta_{1,j}R_{13,j} + \Delta_{2,j}R_{23,j} & -ik_{4,j}\Delta_{1,j}R_{14,j} + \Delta_{2,j}R_{24,j} \\ -ik_{1,j}\Delta_{3,j}R_{21,j}e^{-k_{1,j}L_j} & -ik_{2,j}\Delta_{3,j}R_{22,j}e^{-k_{2,j}L_j} & -ik_{3,j}\Delta_{3,j}R_{23,j} & -ik_{4,j}\Delta_{3,j}R_{24,j} \end{bmatrix} \quad (19)$$

where $\Delta_{1,j} = \left(2\mu_j + \lambda_j \right) A_j$, $\Delta_{2,j} = \lambda_j A_j$ and $\Delta_{3,j} = \mu_j I_j S_1$. The dynamics stiffness matrix $\mathbf{K}_{\omega_n,j}$ can be obtained by $\mathbf{T}_{2,j} \mathbf{T}_{1,j}^{-1}$.

2.3 Throw-off element for modeling semi-infinite and infinite beams

Different to the conventional finite element method, the frequency domain spectral finite element method allows modeling semi-infinite and infinite beams. This section presents a formulation of a throw-off element for simulating a non-reflecting boundary condition for wave propagation problems. In this study guided wave is generated by a transient excitation and then propagates from the excitation location with no secondary disturbances. For a very long beam, the guided wave reflection from boundaries can be neglected because of attenuation after a long travel distance and/or the wave does not research the location under consideration within the time of observation. Considering a throw-off spectral element with a non-reflecting boundary at right end of the beam, the unknown constant $C_{3,j}$ and $C_{4,j}$ in Eq. (9) can be neglect as they represent the wave propagating in the direction toward left end of the beam. The matrix $\mathbf{T}_{1,j}$ and $\mathbf{T}_{2,j}$ can then be reduced to

$$\mathbf{T}_{1,j} = \begin{bmatrix} R_{11,j} & R_{12,j} \\ R_{21,j} & R_{22,j} \end{bmatrix} \quad (20)$$

$$\mathbf{T}_{2,j} = \begin{bmatrix} ik_{1,j}\Delta_{1,j}R_{11,j} - \Delta_{2,j}R_{21,j} & ik_{2,j}\Delta_{1,j}R_{12,j} - \Delta_{2,j}R_{22,j} \\ ik_{1,j}\Delta_{3,j}R_{21,j} & ik_{2,j}\Delta_{3,j}R_{22,j} \end{bmatrix} \tag{21}$$

The dynamics stiffness matrix for the throw-off element can be obtained by $\tilde{\mathbf{K}}_{\omega_n,j} = \mathbf{T}_{2,j}\mathbf{T}_{1,j}^{-1}$.

2.2 Modeling damaged beams

With the throw-off element described in the Section 2.1, a damaged semi-infinite beam is modeled using three spectral finite elements and a throw-off element. The throw-off element is located at the right end of the beam, and hence, no wave is reflected from the right beam end. In this study a step damage is modeled by reducing the cross-sectional area of a beam region with length d_L. The location of the damage L_d is defined as the distance between the left end of the step damage and the left beam end. The cross-section area reduction of the damage can be calculated based on the depth d_d of the step damage as $b(h - d_d)$. The step damage is parameterized by L_d, d_L and d_d, which control the damage location, length and depth. This damaged beam model will then be employed to identify the damage in Section 3 following a probabilistic approach.

3. PROBABILISTIC DAMAGE IDENTIFICATION APPROACH

A probabilistic approach is proposed to identify damages based on measured longitudinal guided wave data. The approach treats the damage parameters described in Section 2 as unknowns parameters and identify them by minimizing the discrepancy between the simulated and measured data. The proposed probabilistic approach not only determines the damage location, length and depth of the damage in beams but also quantifies the uncertainties associated with the damage identification results.

The proposed probabilistic approach follows the Bayesian statistical identification framework (Beck & Katafygiotis 1998). The framework embeds a class of deterministic structural model M within a class of probability model $P(\sigma)$. σ is a prediction-error model parameter. In this study the deterministic structural model M is the damaged frequency domain spectral finite element beam model. The framework allows longitudinal guided wave responses prediction $u(t;\boldsymbol{\theta})$ and modeling of prediction error $e(t,\boldsymbol{\theta})$, which is defined as the difference between the predicted and measured guided wave responses $\tilde{u}(t)$, and is mainly due to the measurement noise and modelling error. It is assumed that the prediction errors are spatially and temporally independent, and normally distributed, and hence, the prediction error is a Gaussian distribution. This assumption allows for a single prediction error parameter σ, corresponding to the standard deviation of the assumed Gaussian distribution. Using the Bayes' theorem, the posterior probability density function (PDF) of the uncertain parameter vector $\mathbf{a} = \{\boldsymbol{\theta}^T, \sigma\}^T \in S(\mathbf{a})$ for a given set of measured guided wave data D and a given class of structural models M can be calculated as

$$p(\mathbf{a}\,|\,D,M) = cp(D\,|\,\mathbf{a},M)\,p(\mathbf{a}\,|\,M) \tag{22}$$

where c is a normalizing constant to ensure the left-hand side of Eq. (22) is equal to unity. $p(\mathbf{a}\,|\,M) = \pi(\mathbf{a})$ is the prior PDF of $\mathbf{a}$ over the set of possible parameter values $S(\mathbf{a})$. The prior PDF is used to reflect the engineer's judgement on the relative plausibility of different values in the parameters. $p(D\,|\,\mathbf{a},M)$ is the likelihood of observing the data given the parameters $\mathbf{a}$ and is defined as

$$p(D\,|\,\mathbf{a},M) = \left(\sqrt{2\pi}\sigma\right)^{-N_t N_o} \exp\left[-\frac{1}{2\sigma^2} \sum_{n=1}^{N_t} \left\| \tilde{u}(t) - u(t;\boldsymbol{\theta}) \right\|^2 \right] \tag{23}$$

where N_o is the number of measurement points. N_t is the number of measured time steps. $\|\cdot\|$ denotes the standard Euclidean norm of the second kind. In practical situation, there exists some uncertainties related to the Young's modulus of the material. Thus the unknown parameter vector $\boldsymbol{\theta}$ in $\mathbf{a}$ contains damage location L_d, length d_L, depth d_d and Young's modulus E.

Using the proposed probabilistic approach to identify the damage, the posterior PDF of the unknown parameters need to be obtained and it can be calculated by integrating Eq. (22) over σ as

$$p(\boldsymbol{\theta}\,|\,D,M) = \int_0^\infty cp(D\,|\,\boldsymbol{\theta},\sigma,M_P)\,\pi(\boldsymbol{\theta},\sigma)d\sigma \tag{24}$$

where $\pi(\mathbf{a})$ is a slowly varying function of σ. In guided wave problem the number of time step in the measured data is usually very large, and hence, the value of $p(\boldsymbol{\theta}\,|\,D,M)$ becomes negligible everywhere except the region of the parameter space where the posterior PDF of the damage parameters is close to its global maximum value. Using the asymptotic approximation (Papadimitriou et al. 1997), Eq. (24) can be approximated as

$$p(\boldsymbol{\theta}\,|\,D,M_P) = c_1 J(\boldsymbol{\theta})^{(N_t N_o - 1)/2}\,\pi(\boldsymbol{\theta}, \hat{\sigma}(\boldsymbol{\theta})) \tag{25}$$

where c_1 is another normalizing constant. $J(\boldsymbol{\theta})$ is a measure-of-fit function between the simulated and measured guided wave signals and is defined as

$$\hat{\sigma}^2(\boldsymbol{\theta}) = J(\boldsymbol{\theta}) = \frac{1}{N_t N_0} \sum_{t=1}^{N_t} \left\| \tilde{u}(t) - u(t;\boldsymbol{\theta}) \right\|^2 \tag{26}$$

The damage identification is achieved by maximizing the posterior PDF $p(\boldsymbol{\theta}\,|\,D,M)$ in Eq. (25), which is equivalent to minimize the $J(\boldsymbol{\theta})$ function. $\hat{\sigma}^2$ is the optimal variance in the prediction error model. In this study a hybrid particle swarm optimization approach, which combines the particle swarm optimization algorithm (Kennedy &

Eberhart 1995) and simplex search method, is employed to solve the optimization problem. Once the optimal parameters are determined, the associated uncertainties can be quantified by the posterior PDF, which can be approximated by a weighted sum of Gaussian distributions centered at R optimal points as

$$p\left(\mathbf{\theta} \mid D, M_P\right) \approx \sum_{r=1}^{R} \frac{\pi\left(\hat{\mathbf{\theta}}^{(r)}\right)\left|\mathbf{A}_N\left(\hat{\mathbf{\theta}}^{(r)}\right)\right|^{-1/2}}{\sum_{r=1}^{R} \pi\left(\hat{\mathbf{\theta}}^{(r)}\right)\left|\mathbf{A}_N\left(\hat{\mathbf{\theta}}^{(r)}\right)\right|^{-1/2}} \mathbf{N}\left(\hat{\mathbf{\theta}}^{(r)}, \mathbf{A}_N^{-1}\left(\hat{\mathbf{\theta}}^{(r)}\right)\right) \tag{27}$$

where $\mathbf{A}_N^{-1}$ is the inverse of Hessian matrix of the function $g(\mathbf{\theta}) = \ln J(\mathbf{\theta})(N_t N_o - 1)/2$ evaluated at r-th optimal point $\hat{\mathbf{\theta}}^{(r)}$ for $r = 1,...,R$. $\mathbf{N}(\mathbf{\mu}, \mathbf{\Sigma})$ denotes a multivariate Gaussian distribution with mean $\mathbf{\mu}$ and covariance matrix $\mathbf{\Sigma}$.

4. EXPERIMENTAL VERIFICATION

4.1 Experimental setup

In this study the proposed damage identification approach was verified using aluminum beams (Grade 6060-T5). The length of the beams was 2 m with 12×6 mm^2 rectangular cross section. A $12 \times 6 \times 2$ mm^3 piezoceramic transducer was adhesively bonded to a beam end to generate the longitudinal guided wave. To enhance the excitability, a $12 \times 6 \times 4$ mm^3 backing mass made by brass was attached to the piezoceramic transducer. The excitation signal was an 80 kHz narrow-band eight-cycle sinusoidal tone burst pulse modulated by a Hanning window. Fig. 1 shows the excitation signal in time and frequency domain.
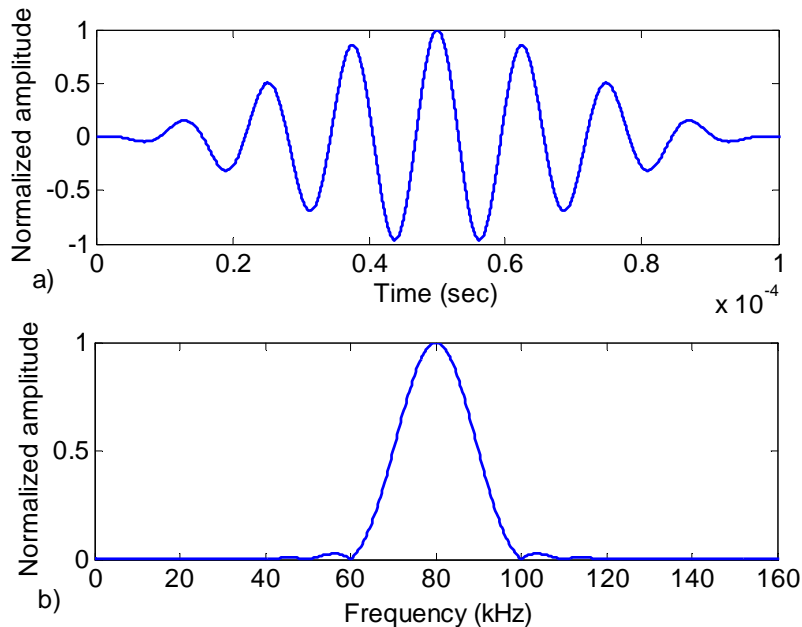

Fig. 1 Eight-cycle 80 kHz sinusoidal excitation signal modulated by a Hanning window in a) time and b) frequency domain

The signal was generated by a computer controlled signal generator (Stanford Research DS345) with 10 V peak-to-peak output voltage and was then amplified 10-50 times through a signal amplifier (Krohn Hite model 7500) before sending the piezoceramic transducer. A one-dimensional laser Doppler vibrometer (Polytech OFV 303/OFV 3001) was employed to measure the longitudinal guided wave signals at 450 mm from the excitation location. The measurement point was centred at the shorter side of the beam cross section to measure the out-of-plane motion due to the Poisson effect of the longitudinal guided wave. A schematic diagram of the experimental setup is shown in Fig. 2. Finally, the measured signals were fed into a computer via an oscilloscope. The signal-to-noise ratio was improved by averaging the signals over a number of acquisitions.
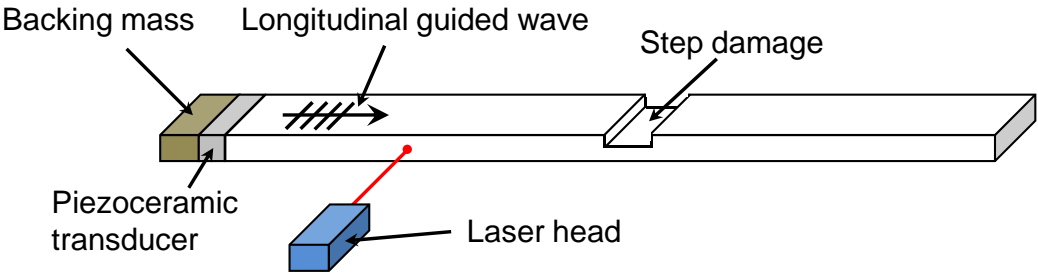

Fig. 2 Schematic diagram of the experimental setup

4.2 Experimental case studies

Two cases were considered in the experimental case studies to verify the proposed damage identification approach. Case C1 considered a step damage located at $L_d =$ 1062.50 mm with 75.00 mm damage length and 2.00 mm damage depth. Case C2 considered a damage with smaller damage depth ($d_d = 1.10$ mm) and was located at $L_d = 915.00$ mm with 90.00 mm damage length. Table 1 provides a summary of all damage cases. The duration of the measured data is 7×10^{-4} s, which allows monitoring a 1 m long region from the measurement location.

Table 1. Summary of all the damage cases in the experimental case studies

Case	Damage location (L_d) (mm)	Damage length (d_L) (mm)	Damage depth (d_d) (mm)
C1	1062.50	75.00	2.00
C2	915.00	90.00	1.10

The proposed damage identification approach described in Section 3 was not only employed to characterize the damage in each case but also quantified the uncertainties associated with the damage identification results. The damage identification results are summarized in Table 2. The predicted damage location, length and depth for Case C1

are 1045.50 mm, 69.71 mm and 2.03 mm, respectively. The corresponding prediction errors are only 1.60%, 7.05% and 1.50%. The results show that the proposed damage identification approach is able to accurately characterize the damage. Case C2 considered a smaller damage depth than Case C1. The reflected longitudinal guided wave amplitude in Case C2 is smaller than that in Case C1. It is expected that it is more challenging to identify the damage in Case C2. The predicted damage location, length and depth for Case C2 are 902.88 mm, 87.46 mm and 1.02 mm. The prediction errors for these damage parameters are 1.33%, 2.82% and 7.00%, respectively. Overall, the proposed damage identification approach is able to accurately identifying the damage in all cases.

Table 2. Summary of the results in damage identification

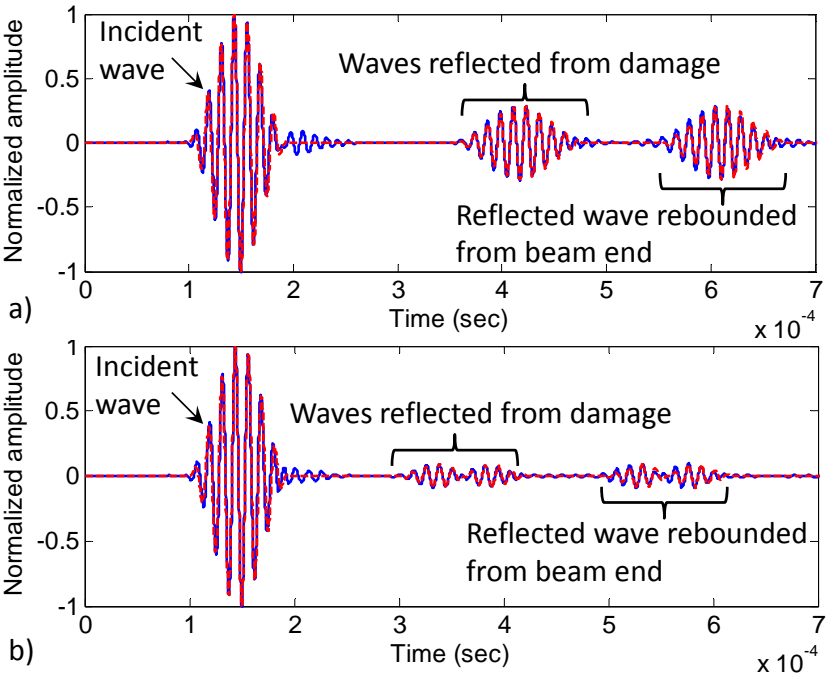| Case	Damage location (L_d) (mm)	Damage length (d_L) (mm)	Damage depth (d_d) (mm)
C1	1045.50 (0.0067%)	69.71 (0.1381%)	2.03 (0.5733%)
C2	902.88 (0.0123%)	87.46 (0.1267%)	1.02 (1.6179%)

Note: value in bracket is the coefficient of variation (COV)

Fig. 3 Comparison of the measured data and the simulated signals from the damaged beam models with the identified parameter vector $\boldsymbol{\theta}$ for a) Cases C1 and b) C2 (sold lines: simulated signals; dashed lines: measured data)

Fig 3 shows a comparison of the measured data and the simulated signals from the damaged beam models with the identified parameter vector θ for Cases C1 and C2. The first pulse is the incident wave. The second and third pulses are the waves reflected from damage and reflected wave rebounded from the left beam end. These figures show that the simulated signals perfectly match the measured data, which indicates the high accuracy of the damage identification.

As discussed in Section 3, the damage identification approach was developed based on the Bayesian statistical framework, in which the uncertainties are quantified by determining the posterior PDF of each damage parameter. As it is not possible to plot a figure with more than three dimensions, Fig. 4a and 4b only show the normalized marginal PDF of the identified damage length and depth, which were calculated by integrating the PDF with respect to other identified parameters, for Cases C1 and C2, respectively. The axes in these figures are plotted at the same scale to enable direct comparison. In this study a non-informative prior distribution was used in the Bayesian statistical framework to calculate the posterior PDF, and hence, the results depend only on the measured data. Both figures show that the PDF value drops shapely for small deviations from the identified damage length. For damage depth, it is obvious that the PDF value for small deviations drops more slowly from the identified damage depth. This means the confidence level of the identified damage depth is lower than the identified damage length.
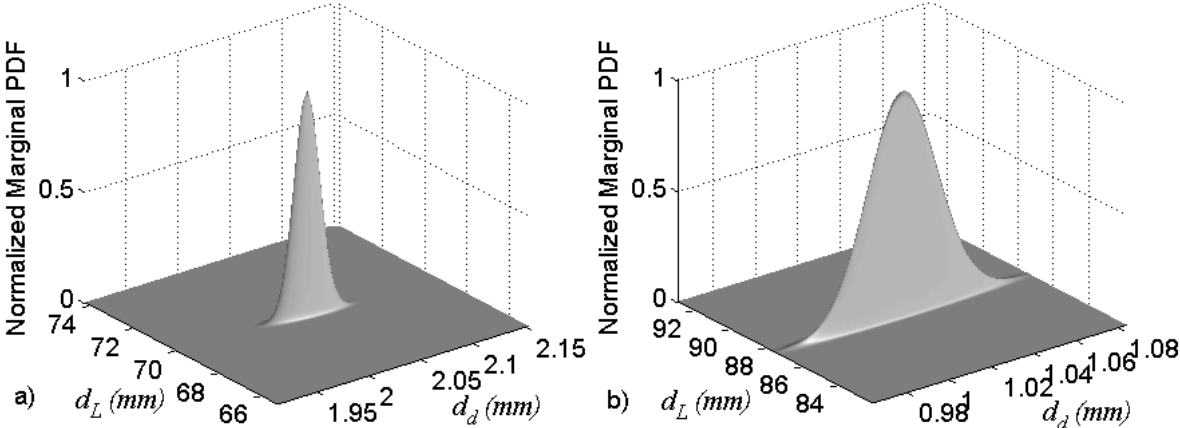

Fig. 4 Normalized marginal PDF of the identified damage length and depth for a) Case C1 and b) C2

The results were also confirmed by calculating the coefficient of variation (COV) of the damage identification results. The results of the all identified damage parameters are shown in Table 2. The COV values indicate that the confident level of the identified damage location is always very high given the fact that the guided wave is very

sensitive to the damage location. However, the confident level of the identified depth is generally the lowest among the identified damage parameters.

5. CONCLUSIONS

This paper has presented an experimental study of identifying damages in beams using a probabilistic approach. Longitudinal guided wave measured at a single point on the beams was employed as the signal to identify the location, length and depth of the step damage. In addition to identifying the damages, the proposed approach also quantified the uncertainties associated with the damage identification results. In the experimental study a piezoceramic transducer was used for exciting the longitudinal guided wave. The wave signals were then measured using a one-dimensional laser Doppler vibrometer. Metallic beams with two different damage configurations were considered in the experimental case studies. They demonstrated the capability of the proposed damage identification approach. Overall the proposed approach is able to accurately identify the damages. The work is currently underway to consider comprehensive experimental case studies to fully verify the proposed damage identification approach.

Acknowledgement

REFERENCES

Beck, J.L. and Katafygiotis, L.S. (1998). "Updating models and their uncertainties I: Bayesian statistical framework", J. Eng. Mech. ASCE, **124**, 455-461.

Doyle, J.F. (1997), "Wave propagation in structures spectral analysis using fast discrete Fourier transforms, second edition, Springer.

Jean-Pierre, D. and Tisseur, F. (2003). "Perturbation theory for homogeneous polynomial eigenvalue problem", Linear Algebra & Its Apps., **358**, 71-94.

Kennedy, J. and Eberhart, R.C. (1995). "Particle swarm optimization", Proceedings of IEEE Inter. Conf. Neural Networks IV, Piscataway, IEEE, 1942-1948.

Kim, H. and Melhem, H. (2004). "Damage detection of structures by wavelet analysis", Engineering Structures, **26**, 347-362.

Krawczuk, M. (2002). "Application of spectral beam finite element with a crack and iterative search technique for damage detection", Finite Elem. Analy. Design, **38**, 537-548.

Krawczuk, M., Grabowska, J. and Palacz, M. (2006). "Longitudinal wave propagation Part I – Comparison of rod theories", J. Sound Vib., **295,** 461-478.

Lam, H.F., Ng, C.T. and Leung, A.Y.T. (2008). "Multicrack detection on semirigidly connected beams utilizing dynamic data", J. Eng. Mech. ASCE, **134**, 90-99.

Liew, C.K. and Veidt, M. (2009). "Pattern recognition of guided waves for damage evaluation in bars", Pattern Recog. Letters, **30**, 321-330.

Nag, A. Roy Mahapatra, D. and Gopalakrishnan, S. (2002). "Identification of delamination in composite beams using spectral estimation and a genetic algorithm", Smart Mater. Struct., **11**, 899-908.

Ng, C.T. and Veidt, M. (2011). "Scattering of the fundamental anti-symmetric Lamb wave at delamination sin composite laminates", J. Acoust. Soc. Am., **129**, 1288-1296.

Ng, C.T., Veidt, M. and Lam, H.F. (2009). "Guided wave damage characterisation in beams utilising probabilistic optimisation", Eng. Struct., **31**, 2842-2850.

Papadimitriou, C., Beck, J.L., and Katafygiotis, L.S. (1997), "Asymptotic expansions for reliability and moments of uncertain systems", J. Eng. Mech. ASCE, **123,** 1219-1229.

Pau, A. and Vestroni, F. (2011). "Wave propagation in one-dimensional waveguides for damage characterization", J. Intell. Mater. Syst. Struct. **22**, 1869-1877.

Rosales, M.B., Filipich, C.P. and Buezas, F.S. (2009). "Crack detection in beam-like structures", Engineering Structures, **31**, 2257-2264.

Rucka, M. (2010). "Experimental and numerical studies of guided wave damage detection in bars with structural discontinuities", Archive App. Mech., **80**, 1371-1390.

Veidt, M. and Ng, C.T. (2011). "Influence of stacking sequence on scattering characteristic of the fundamental anti-symmetric Lamb wave at through holes in composite laminates", J. Acoust. Soc. Am., **129**, 1280-1287.